THE JOURNAL OF BIOLOGICAL CHEMISTRY VOL. 292, NO. 15, pp. 6225–6239, April 14, 2017

Pathogenic mutations in retinitis pigmentosa 2 predominantly result in loss of RP2 protein stability in humans and zebrafish

Received for publication, September 25, 2016, and in revised form, February 14, 2017 Published, JBC Papers in Press, February 16, 2017, DOI 10.1074/jbc.M116.760314

Fei Liu[‡1], Yayun Qin[‡1], Shanshan Yu[‡1], Dinesh C. Soares[§1], Lifang Yang[‡], Jun Weng[‡], Chang Li[‡], Meng Gao[‡], Zhaojing Lu[‡], Xuebin Hu[‡], Xiliang Liu[‡], Tao Jiang[‡], Jing Yu Liu[‡], Xinhua Shu[¶], Zhaohui Tang[‡], and Mugen Liu[‡2]

From the [‡]Key Laboratory of Molecular Biophysics of Ministry of Education, Department of Genetics and Developmental Biology, College of Life Science and Technology, Huazhong University of Science and Technology, Wuhan, Hubei 430074, China, [§]MRC Human Genetics Unit/Centre for Genomic and Experimental Medicine, MRC Institute of Genetics and Molecular Medicine, University of Edinburgh, Edinburgh EH4 2XU, United Kingdom, and [¶]Department of Life Sciences, Glasgow Caledonian University, Glasgow G4 0BA, United Kingdom

Edited by Xiao-Fan Wang

Mutations in retinitis pigmentosa 2 (*RP2*) account for 10–20% of X-linked retinitis pigmentosa (RP) cases. The encoded RP2 protein is implicated in ciliary trafficking of myristoylated and prenylated proteins in photoreceptor cells. To date >70 mutations in *RP2* have been identified. How these mutations disrupt the function of RP2 is not fully understood. Here we report a novel in-frame 12-bp deletion (c.357_368del, p.Pro120_Gly123del) in zebrafish *rp2*. The mutant zebrafish shows reduced rod phototransduction proteins and progressive retinal degeneration. Interestingly, the protein level of mutant Rp2 is almost undetectable, whereas its mRNA level is near normal, indicating a possible post-translational effect of the mutation. Consistent with this hypothesis, the equivalent 12-bp deletion in human *RP2* markedly impairs RP2 protein stability and reduces its protein level. Furthermore, we found that a majority of the *RP2* pathogenic mutations (including missense, single-residue deletion, and C-terminal truncation mutations) severely destabilize the RP2 protein. The destabilized RP2 mutant proteins are degraded via the proteasome pathway, resulting in dramatically decreased protein levels. The remaining non-destabilizing mutations T87I, R118H/R118G/R118L/R118C, E138G, and R211H/R211L are suggested to impair the interaction between RP2 and its protein partners (such as ARL3) or with as yet unknown partners. By utilizing a combination of *in silico*, *in vitro*, and *in vivo* approaches, our work comprehensively indicates that loss of RP2 protein structural stability is the predominating pathogenic consequence for most *RP2* mutations. Our study also reveals a role of the C-terminal domain of RP2 in maintaining the overall protein stability.

Retinitis pigmentosa (RP,[3] OMIM #268000) is a group of inherited retinal degenerative diseases characterized by progressive loss of photoreceptor function. RP affects ~1 in 4000 individuals worldwide (1). Typically, RP patients undergo night blindness, gradually worsening vision from the periphery to the center, and even complete blindness. Currently no therapy can effectively relieve the vision loss caused by RP.

Mutations in the retinitis pigmentosa 2 (*RP2*) gene alone represent the genetic causes of 10–20% of X-linked retinitis pigmentosa (XLRP) families (2, 3). Human *RP2* encodes a ubiquitously expressed polypeptide of 350 amino acids and is well conserved across different vertebrate species including mouse (88% identity) and zebrafish (67% identity). Knock-out of the orthologs of *RP2* in mice (4–6) and zebrafish (7) indeed lead to progressive retinal degeneration, suggesting a crucial role of RP2 protein in maintaining the normal functions of the retina.

The RP2 protein contains two domains, an N-terminal tubulin folding cofactor C-like (TBCC) domain (residues ~42–192) and a C-terminal nucleoside diphosphate kinase-like (NDPK) domain (residues ~251–346) (8–12). Two proteins, the ADP-ribosylation factor like GTPase 3 (ARL3) (12, 13) and the G protein subunit β1 (GNB1, β subunit of rod transducin) (14), are known to interact with the N-terminal TBCC domain of RP2. By acting as a GTPase-activating protein (GAP) specifically for ARL3, RP2 plays a role in the ciliary trafficking of myristoylated and prenylated proteins (5, 15–17). Binding of RP2 to GNB1 also facilitates the membrane association and traffic of GNB1 probably in an ARL3-independent manner (14). The pathogenic mutations R118H and E138G drastically reduce the affinity of RP2 to ARL3 (11, 12), suggesting loss of this interaction might be correlated with the occurrence of RP. The C-terminal NDPK domain of RP2 shows sequence and structure similarity to the nucleotide diphosphate kinases. Nevertheless, due

This work was supported by the National Natural Science Foundation of China (81670890, 31601026, 81500762, 31571303, 31471194, and 81371064) and the China Postdoctoral Science Foundation (2015M582216). The authors declare that they have no conflicts of interest with the contents of this article.
This article contains supplemental Table S1 and Figs. S1–S8.
[1] Joint first authors.
[2] To whom correspondence should be addressed: Dept. of Genetics and Developmental Biology, College of Life Science and Technology, Huazhong University of Science and Technology, Wuhan 430074, China. Tel.: 86 2787794549; Fax: +86 2787794549; E-mail: lium@hust.edu.cn.

[3] The abbreviations used are: RP, retinitis pigmentosa; TBCC, tubulin folding cofactor C-like; NDPK, nucleoside diphosphate kinase-like; ARL3, ADP-ribosylation factor like GTPase 3; GNB1, G protein subunit β1; GAP, GTPase-activating protein; TALEN, transcription activator-like effector nuclease; PNA, peanut lectin; DSF, differential scanning fluorimetry; NSF, *N*-ethylmaleimide-sensitive factor; WB, Western blot; RT-qPCR, quantitative reverse transcription PCR.

to the variations around the active site, it is unlikely that RP2 protein has kinase activity (11, 18). The physiological functions of this domain remain unclear.

To date, >70 pathogenic mutations in *RP2* have been identified (Human Gene Mutation Database) (19). More than ⅔ of these mutations are predicted to result in C-terminal truncated RP2 proteins or the complete loss of the *RP2* gene. The most common truncation mutation, Arg120Ter, has been reported to cause loss of the entire RP2 protein, probably due to nonsense-mediated mRNA decay (20, 21). The remaining mutations in *RP2* are missense or small in-frame deletions. With the exception of R118H and E138G, little is known about the effects of these mutations on the structure and function of RP2 protein.

In the present study we obtained a novel *rp2* mutant zebrafish line carrying a 12-bp in-frame deletion mutation (4-residue deletion at protein level) generated by the transcription activator-like effector nuclease (TALEN) technology. The retinal phenotype and molecular etiology of the novel *rp2* mutant zebrafish was determined. Furthermore, we revealed that like the 12-bp deletion identified in zebrafish *rp2*, most of the missense and C-terminal truncation mutations identified in RP2 patients destabilized the RP2 protein and caused protein degradation through the proteasome pathway.

Results

The del12 mutation causes loss of Rp2 protein in zebrafish

We previously reported the generation of *rp2* knock-out zebrafish by TALEN technology that resulted in a frameshift mutation (c.359_363del, named del5) causing null allele of *rp2* (7). In this study we identified a novel *rp2* mutant zebrafish line carrying a 12-bp in-frame deletion (c.357_368del, named del12). The del12 mutation is predicted to cause deletion of four-conserved amino acid residues (Pro-120, Val-121, Lys-122, and Gly-123) located in the TBCC domain of Rp2 at the protein level. Homozygotes were screened out and confirmed by DNA sequencing (Fig. 1*A*). Like the *rp2* knock-out zebrafish (7), the del12 homozygous mutants did not show any apparent developmental defects and grew and bred normally.

Intriguingly, using the anti-zebrafish Rp2 antibody described previously (7), we found that the Rp2 protein levels were reduced to ~10% in del12 homozygotes (Fig. 1*B*) and 60–80% in del12 heterozygotes (supplemental Fig. S1) in Western blot analysis. Furthermore, we examined the localization of Rp2 in WT and del12 mutant retinas at the age of 3 months under dark- and light-adapted conditions. In WT retinas, Rp2 was mainly associated with the plasma membrane of photoreceptor cells from the synapses to the outer segments. But in the del12 mutant retinas, Rp2 signals were much weaker (Fig. 1*C* and supplemental Fig. S2), which is in agreement with the Western blot results.

To test if the loss of Rp2 protein was due to the reduction of *rp2* mRNA, quantitative reverse transcription PCR (RT-qPCR) was performed using WT and mutant (del5 and del12) zebrafish eyes. Unlike the del5 mutant mRNA levels, which were decreased to ~15% of WT group by nonsense-mediated decay, the del12 mutant mRNA levels were slightly reduced to >80% of WT group (Fig. 1*D*). Because the mild reduction of del12 mutant mRNA is unlikely to cause the near complete loss of Rp2 protein, we reasoned that there might be a post-translational mechanism degrading the mutant Rp2 protein.

Reduced rod phototransduction proteins and progressive retinal degeneration in del12 mutant zebrafish

As the del12 mutants showed very low levels of Rp2 protein, we speculated that the normal function of Rp2 might be abolished or at least impaired. To validate this we first chose several proteins that had been studied in the *rp2* knock-out zebrafish (7) and detected their protein levels in WT and del12 mutant zebrafish by Western blot. The prenylated Pde6b and Grk1 and the myristoylated Gnat1, which participate in the phototransduction process of rod cells, are candidate trafficking substrates regulated by the RP2-ARL3 complex (22). All of them were down-regulated in the del12 mutants at the ages of 1 month (Fig. 2*A*) and 2 months (Fig. 2*B*). The degrees of down-regulation of the three proteins in the del12 mutants were similar to those of the *rp2* knock-out (del5) zebrafish. GNB1 and GNB3 are the β subunit of the rod and cone transducin complex, respectively. RP2 interacts with GNB1 but not GNB3 (14). In the del12 mutant zebrafish, the protein levels of Gnb1 were reduced, whereas Gnb3 levels were unchanged. Additionally, we checked the expression of two other Rp2-interacting proteins, Arl3 and Nsf (23). Their protein levels were unaffected in both *rp2* mutant zebrafish lines (Fig. 2, *A* and *B* and supplemental Fig. S1).

To assess the retinal phenotype of the del12 mutant zebrafish, we used the peanut lectin (PNA) and the anti-rhodopsin (4D2) antibody to label the outer segments of cones and rods, respectively. At the age of 6 months, the outer segments of rods in del12 mutant zebrafish showed a reduction in length as compared with WT zebrafish, whereas the outer segments of cones were mildly affected (Fig. 2*C*). Furthermore, we performed transmission electron microscopy assays on the retinas of 7-month-old WT and del12 mutant zebrafish. The del12 mutant zebrafish also showed shortened outer segments of photoreceptors when compared with WT (Fig. 2*D*). These results suggest that the del12 mutant zebrafish exhibits similar molecular defects and retinal phenotypes observed previously in the *rp2* knock-out zebrafish (7).

The equivalent del12 mutation in human RP2 decreases its protein level and stability

The four residues affected by the del12 mutation are identical between human and zebrafish RP2 proteins. We constructed an equivalent del12 mutation by deleting the corresponding four residues (Pro-95, Val-96, Lys-97, and Gly-98) in human *RP2* and then expressed the WT and del12 mutant RP2 protein with a C-terminal GFP or FLAG tag in ARPE-19 cells. Because the expression was controlled by the CMV promoter, without the 5′- and 3′-UTR of native *RP2* mRNA, the interference of possible regulatory mechanisms acting on mRNA levels was excluded. We found that the protein levels of del12 mutant RP2 were reduced to ~30% (GFP-tagged) and 15% (FLAG-tagged) of WT (Fig. 3, *A* and *B*). We also detected the expression levels of del12 mutant RP2 in two other human cell lines (H1299 and

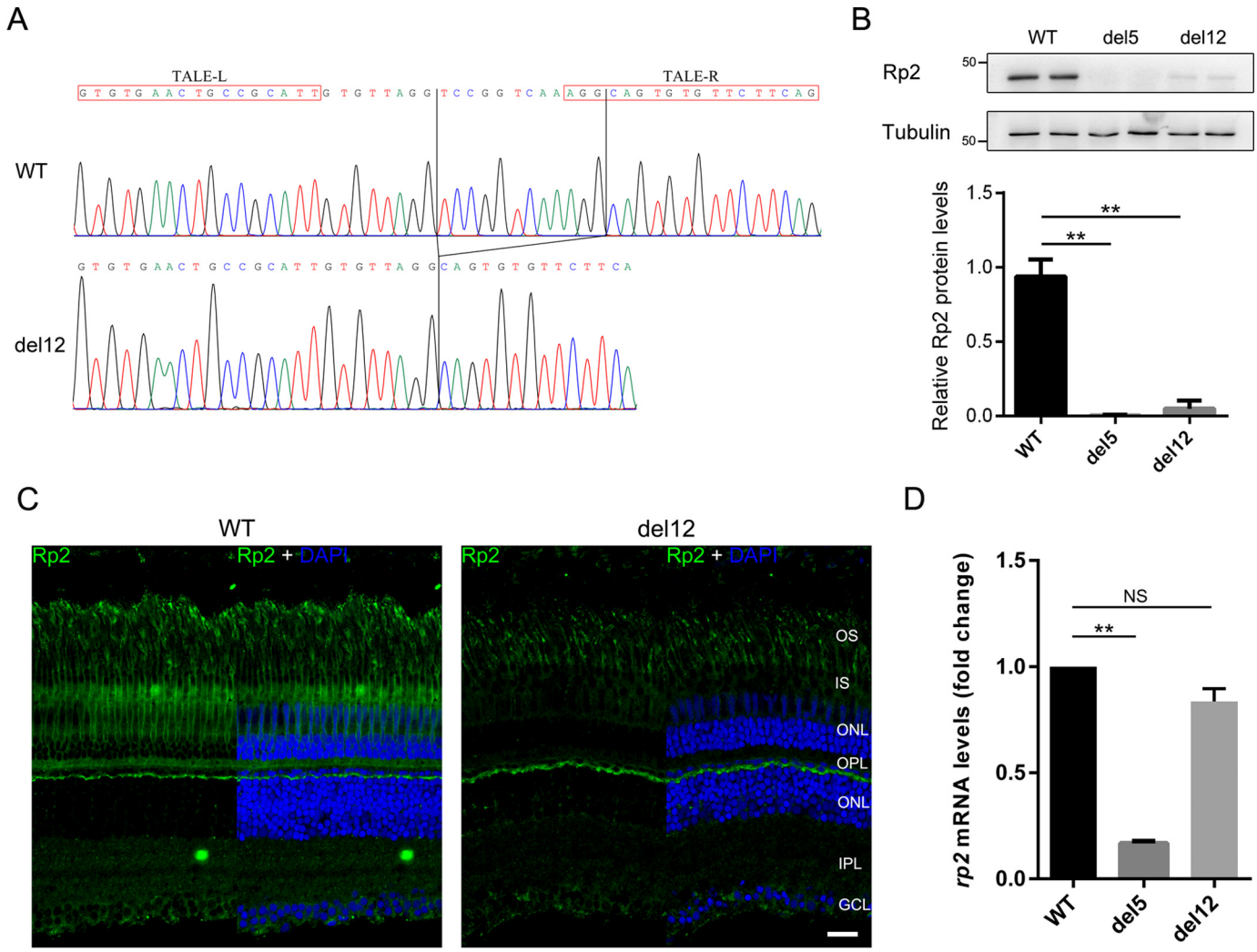

Figure 1. Identification of the del12 mutant zebrafish with dramatically decreased Rp2 protein levels. *A*, the c.357_368del mutation (del12) in zebrafish *rp2* was confirmed by Sanger sequencing at the genomic level. The chromatograms of WT and del12 zebrafish are shown. The TALE binding sequences are marked by *red boxes*. The deleted 12 bp is labeled by *vertical lines*. *B*, protein levels of Rp2 were detected in WT, del5 (knock-out) and del12 mutant zebrafish at the age of 3 months by Western blot using the anti-zebrafish Rp2 antibody. Tubulin served as a loading control. Quantitative results of Rp2 protein levels in del5 and del12 homozygotes from three independent experiments ($n = 6$) are shown as the mean with S.D. in the lower panel. **, $p < 0.01$. *C*, immunostaining of Rp2 in dark-adapted retinas from WT and del12 mutant zebrafish at the age of 3 months. As compared with WT, the del12 mutants show much weaker fluorescent signals in the retina. *OS*, outer segment; *IS*, inner segment; *ONL*, outer nuclear layer; *OPL*, outer plexiform layer; *INL*, inner nuclear layer; *IPL*, inner plexiform layer, *GCL*, ganglion cell layer. Scale bar: 20 μm. *D*, the corresponding *rp2* mRNA levels in 3-month-old WT and *rp2* mutant zebrafish were detected by RT-qPCR. *Actb1* was used as an endogenous control. The results are shown as the mean with S.D. ($n = 3$). **, $p < 0.01$. NS, not significant.

HepG2) and obtained similar results (supplemental Fig. S3). These results suggest that the biological process causing the decrease of the del12 mutant protein is similar in human and zebrafish and present in different cell types.

As the Pro-95 residue was affected by the del12 mutation and a pathogenic mutation in the same codon (P95L) has been identified in RP patients (24), we then examined the expression level of P95L mutant RP2 in ARPE-19 cells. Similar to the del12 mutation, P95L reduced the protein levels of RP2 to ~30% (Fig. 3, *C* and *D*) when compared with WT or the R118H mutation, which does not affect the protein levels (25). Two other nearby pathogenic mutations, C86Y (24) and C108G (20), also showed similar effects on the protein levels of RP2 in the expression experiments (Fig. 3, *C* and *D*). These results suggest that the del12 mutation and the nearby C68Y, P95L, and C108G missense mutations might cause retinal degenerations through a shared mechanism that dramatically decreases the protein levels of RP2.

Crystal structure studies of RP2 revealed that the N-terminal domain of RP2 forms a parallel β-helix (residues 34–192) with a tightly packed and mainly hydrophobic core (11). The Pro-95, Val-96, Lys-97, and Gly-98 affected by the del12 mutation make up part of the β-strand (residues 90–103) that participate in the β-sheet formation within this β-helix domain. Analysis of the intraprotein interactions (26) of the four residues based on the human RP2 crystal structure reveals that these residues support critical β-helix stabilizing main-chain to main-chain hydrogen bonds and hydrophobic interactions that are required for core structural stability of the protein (Fig. 3*E*). For example, Val-96 is involved in main-chain to main-chain H-bonds with the residue Ala-113 in another β-strand. Therefore, deletion of these four residues might compromise

the folding of the parallel β-helix and in turn the overall protein conformation, which would likely cause rapid degradation of the mutant protein.

To substantiate the prediction, we expressed and purified the WT, del12, P95L, and R118H forms of human RP2 protein with an N-terminal GST tag in *Escherichia coli* cells. Under the same conditions the WT and R118H forms of RP2 were mainly soluble and present in the supernatants of cell lysates, whereas the majority of del12 and P95L mutant RP2 formed inclusion bodies in the precipitates (supplemental Fig. S4). Differential scan-

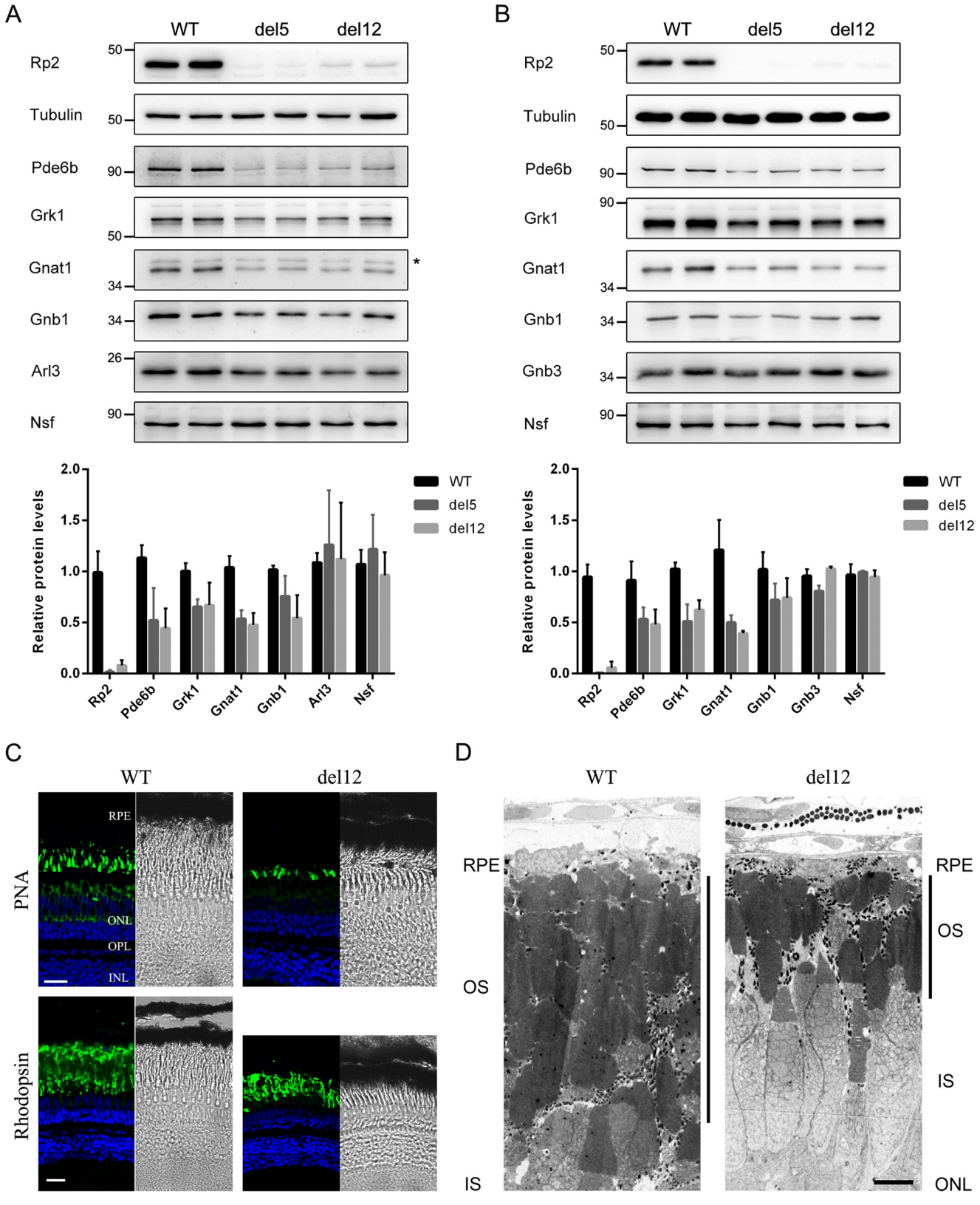

ning fluorometry (DSF) was used to determine the thermal stabilities of the purified RP2 proteins. The R118H group showed similar patterns of fluorescence to the WT group (Fig. 3*F*, *blue* and *green lines*). Meanwhile, the del12 and P95L groups exhibited high initial fluorescence signals at low temperatures (Fig. 3*F*, *red* and *purple lines*), suggesting the proteins were not well folded at all. These results indicate the del12 and P95L mutant RP2 proteins were unstable and more inclined to be unfolded and aggregated than WT RP2 protein.

Over half of the missense and small in-frame deletion mutations in RP2 are destabilizing

To date, >70 pathogenic mutations in *RP2* have been reported in the literature, including 22 missense or small in-frame deletion mutations (19). As the C86Y, P95L, and C108G mutations clearly decrease the protein levels of RP2, we next wanted to know if the remaining *RP2* missense or small in-frame deletion mutations showed similar effects. A total of 19 *RP2* additional mutations (see Fig. 4*A*) were constructed and heterogeneously expressed in ARPE-19 cells. Protein levels of WT and mutant RP2 were detected by Western blot. In summary, 12 mutations, G2V (3), F5del (27), S6del (8), C67Y (28), C86Y, P95L, C105W (3), C108G, I137del (24), S140F (29), L253R (30), and L253P (31) together with the del12 mutation were found to markedly decrease the protein levels of RP2 (Fig. 4, *B* and *C*), suggesting that they are likely destabilizing. On the contrary, 10 mutations, C3S (31), T87I (31), R118H, R118G (2), R118L (9), R118C (32), E138G (9), L188P (28), R211H (3), and R211L (33), showed no or mild effects on the expression levels of RP2 (Fig. 4, *B* and *C*). R282W, which is a non-pathogenic polymorphism (34), was used as a negative control in the study and showed normal RP2 protein levels. Repeated experiments in HepG2 cells showed similar results (supplemental Fig. S5). Using the del12 mutation, which showed protein levels of ~30% of WT in cultured cells (*in vitro*) but <10% in zebrafish (*in vivo*), as a reference, we predicted that patients carrying these mutations should have very low levels of RP2 protein (Fig. 4*C*). These results indicate that for more than half of the missense and small in-frame deletion mutations, loss of RP2 proteins might be the main cause of disease.

We further performed *in silico* stability analysis of these mutations using FoldX (35, 36) to evaluate their effects on the three-dimensional crystal structures of RP2 protein (11, 12) and provide a structural framework for interpreting pathogenicity. A total of 17 missense mutations in *RP2* affecting 12 amino acid residue positions were analyzed (Fig. 5*A*) (note, the two N-terminal missense mutations G2V and C3S are present within a disordered region and not visible in the solved crystal structures). 10 of the 12 positions lie within the N-terminal TBCC domain, whereas one mutation position (Arg-211) lies in the linker region and one (Leu-253) lies in the C-terminal NDPK domain. From the FoldX *in silico* mutagenesis analysis of the unbound RP2 structure (Fig. 5*B* and supplemental Table S1), pathogenic mutations T87I, R118H/R118L/R118C, E138G, and R211H/R211L and polymorphism R282W do not destabilize the protein, as judged by $\Delta\Delta G$ values <1.6 kcal/mol (36). All of these positions are solvent-exposed (Fig. 4*A*, *blue-* or *cyan-labeled*), suggesting they play critical roles in protein-protein interaction, which are otherwise impaired in the mutated RP2 proteins. On the other hand, the buried C67Y, C86Y, P95L, C105W, C108G, S140F, L253R, and L253P (Fig. 4*A*, *white labeled*) are all predicted to severely destabilize the protein ($\Delta\Delta G > 1.6$ kcal/mol) and thus potentially cause degradation of the mutated RP2, which may be interpreted as decreased levels of the expressed mutant proteins (see Fig. 4, *B* and *C*). The FoldX analysis of the Arl3-bound RP2 crystal structure mirrors the results of the unbound structure (supplemental Table S1).

Two mutations, R118G and L188P, were predicted to be destabilizing *in silico* but showed mild effects on the protein levels of RP2 (Fig. 4, *B* and *C*). To investigate these aberrant results more carefully, we performed DSF analysis to directly measure the stabilities of these mutant RP2 proteins. As shown in supplemental Fig. S6, the R118G, E138G, and L188P mutations decreased the protein stabilities of RP2 by ~3 °C, 5 °C, and 11 °C, respectively. The T87I, R118H, and R211H mutant proteins showed no significant differences when compared with WT. In general, the results of expression tests and DSF analysis fit well but not 100 % with the *in silico* prediction.

Truncation mutations causing imperfect C-terminal domain destabilize RP2 protein

Truncation mutations in *RP2* often induce nonsense-mediated mRNA decay and cause loss of the entire protein, such as Arg-120* (37) and Tyr-151* (25). However, when the incorrect termination codon is located very close to the C-terminal end of RP2, the mutant mRNA might escape from nonsense-mediated decay, but still no RP2 protein could be detected (25, 38). In that case the prematurely terminated RP2 protein with an incomplete C-terminal domain, but not the mutant *RP2* mRNA, might be implicated. This prompted us that the C-terminal domain might play a role in stabilizing the RP2 protein. To verify this hypothesis, we constructed a series of C-terminal-truncated RP2 mutants (1–42, 1–192, 1–251, 1–300, 1–330 and 1–340) to mimic the truncation mutations (Fig. 6*A*) and examined their expression levels in ARPE-19 cells.

We found that only the 1–340 of C-terminal truncation showed comparable protein levels as WT (Fig. 6, *B* and *C*). The 1–192 (TBCC domain alone), 1–251 (TBCC domain plus the linker), 1–300, and 1–330 (TBCC domain plus the linker and

Figure 2. The del12 mutant zebrafish showed decreased rod phototransduction proteins and progressive retinal degeneration. *A* and *B*, protein levels of the rod phototransduction proteins (Pde6b, Grk1, Gnat1, and Gnb1) and cone phototransduction protein Gnb3 as well as the two RP2-interacting protein Arl3 and Nsf were detected by Western blot in 1-month-old (*A*) and 2-month-old (*B*) WT, del5, and del12 mutant zebrafish. Tubulin was used as a loading control. The *asterisk* in *A* indicates a nonspecific bands produced by the anti-GNAT1 antibody. The quantitative results are shown as the mean with S.D. ($n = 6$) in the *lower panels*, respectively. *C*, retinal cryosections from WT and del12 mutant zebrafish were stained with PNA (*upper panel*) and the anti-rhodopsin (4D2) antibody (*lower panel*) to label the outer segments of cones and rods at the age of 6 months. Reduction in the thickness of the rod outer segment layer is seen in del12 mutant zebrafish. *Scale bars*: 20 μm. *D*, retinal ultrastructure analysis of 7-month-old WT and del12 mutant zebrafish revealed significantly shortened outer segments of photoreceptors in del12 mutant zebrafish. *RPE*, retinal pigment epithelium; *OS*, outer segment; *IS*, inner segment; *ONL*, outer nuclear layer. *Scale bars*: 5 μm.

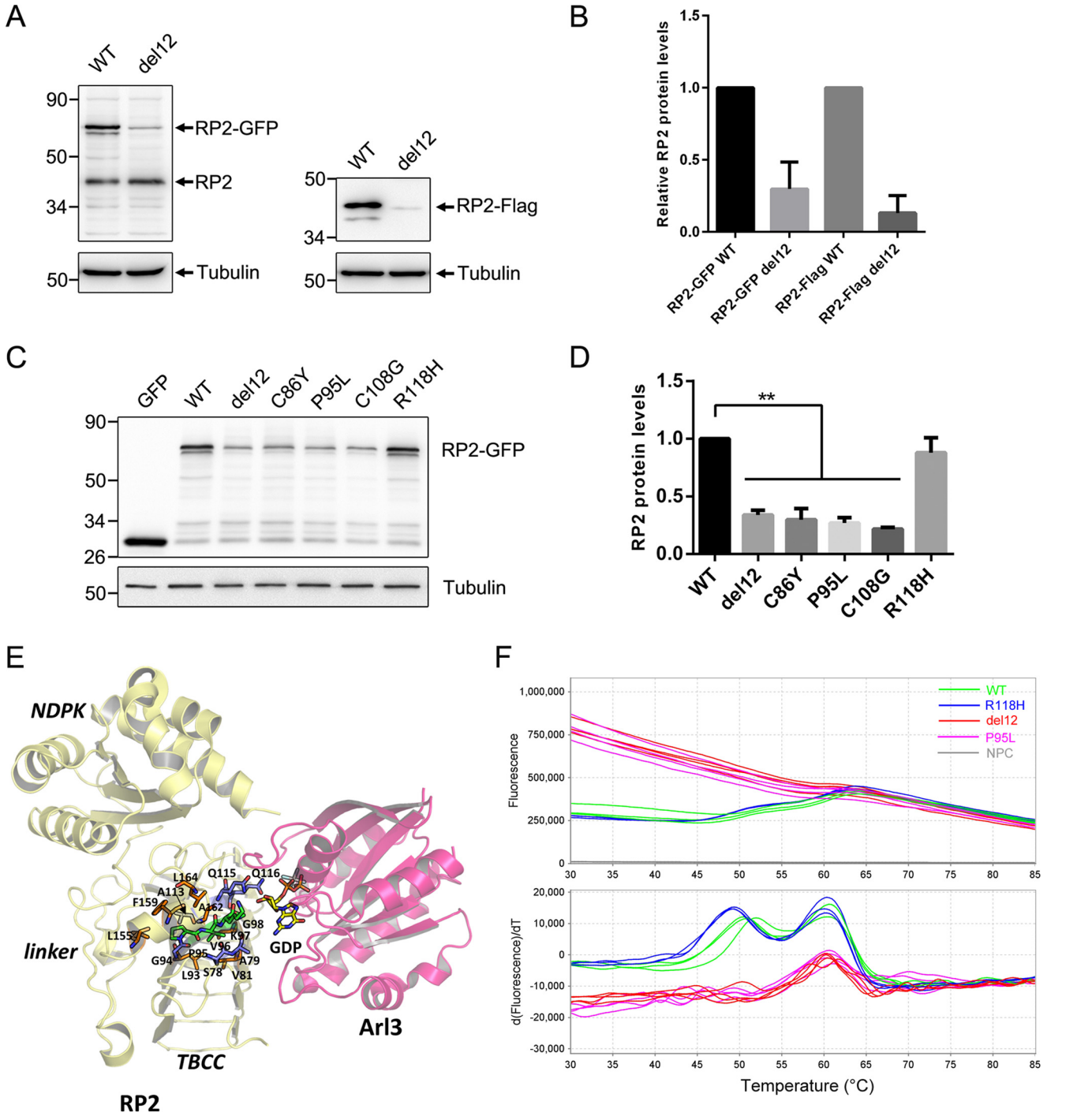

Figure 3. The del12 and nearby mutations in human *RP2* decreased its protein level and stability. *A*, C-terminal GFP or FLAG-tagged WT and del12 mutant RP2 were transfected into ARPE-19 cells. The RP2 protein levels were detected by Western blot using the anti-human RP2 antibody or the anti-FLAG antibody. The endogenous and GFP or FLAG-tagged RP2 bands are indicated by *arrows*. Tubulin was used as a loading control. *B*, the quantitative results of *A* from five independent experiments are shown as the mean with S.D. ($n = 5$). The del12 mutation significantly reduced the protein levels of RP2. *C*, the nearby C86Y, P95L, and C108G mutations of *RP2* show similar effects as the del12 mutation on the expression of RP2 in ARPE-19 cells. The R118H mutation was used as a control. *GFP*, the empty vector without *RP2* sequence. *D*, the quantitative results of *C* from three independent experiments are shown as the mean with S.D. ($n = 3$). **, $p < 0.01$. *E*, intraprotein interactions of the four residues affected by the *RP2* del12 mutation. Pro-95, Val-96, Lys-97, and Gly-98 are shown in stick representation colored *green*. Those residues that participate in H-bonds with the four residues are shown in *blue*, and hydrophobic interactions are in *orange*. *F*, the melting curve plots and derivative plots of WT, del12, P95L, and R118H forms of GST-RP2 fusion proteins in DSF analysis are shown. The high initial fluorescence signals of del12 and P95L groups (*upper panel*, *red* and *purple lines*) indicate that the proteins are partially or completely unfolded at the beginning. The two transitions (around 50 and 60 °C) of WT and R118H groups (*lower panel*, *green* and *blue lines*) represent the unfolding processes of RP2 and GST with increasing temperature, respectively. *NPC*, no protein control.

incomplete NDPK domain) forms of RP2 were unstable. These results suggest that an intact C-terminal domain (longer than 1–330) is essential for the overall stability of RP2. To date, the insertion-deletion mutation c.968delAinsTCC (K323Ifs*8), which results in a premature termination at codon 330, is the closest mutation to the C terminus of RP2 (27). According to

our work and previous studies, patients carrying truncation mutations in *RP2* are unlikely to have normal levels of RP2 protein.

Next, we also examined the N-terminal-truncated RP2 mutants (42–350, 192–350, and 251–350) (Fig. 6*A*). The 192–350 truncation showed a mild decrease of the RP2 protein level in

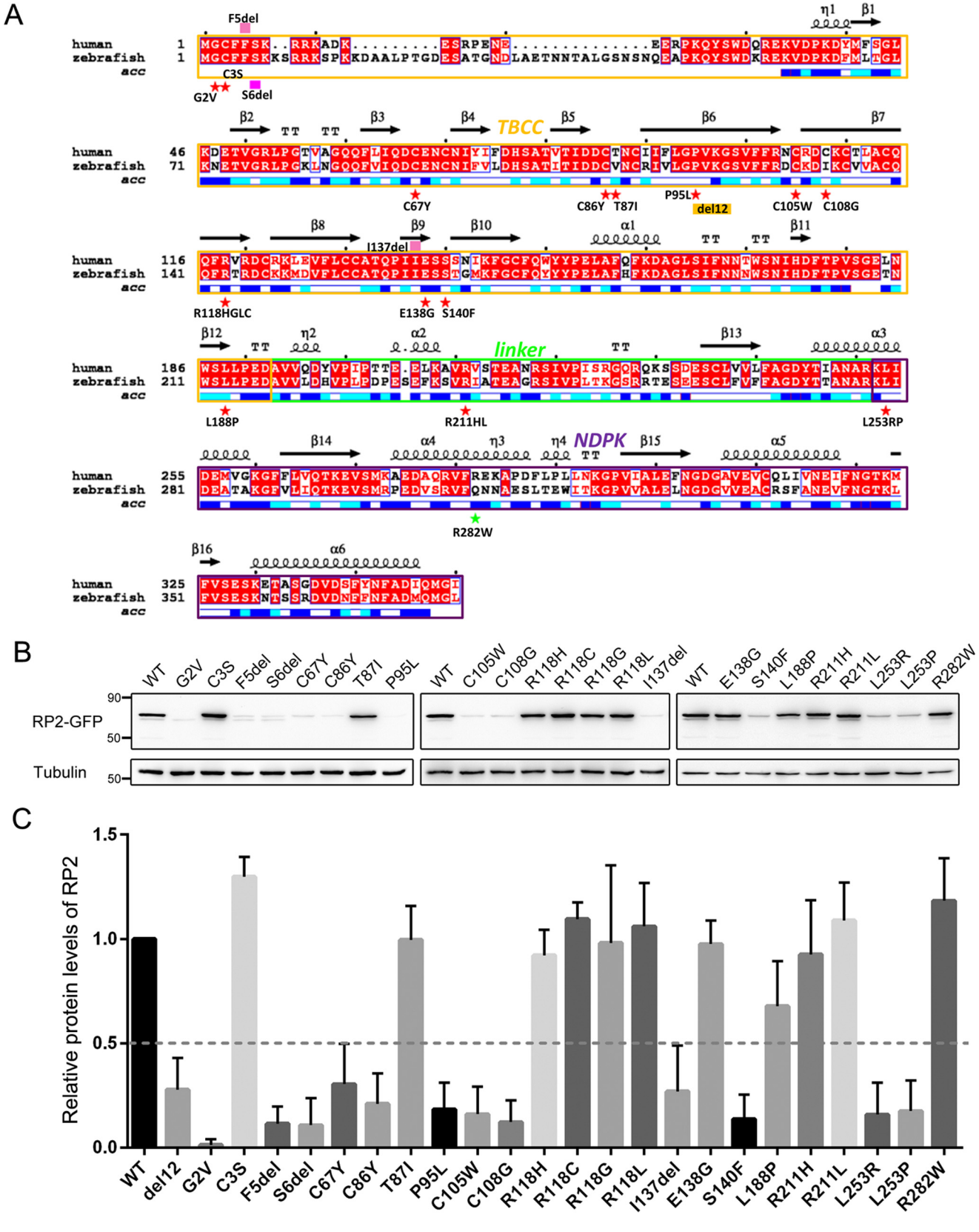

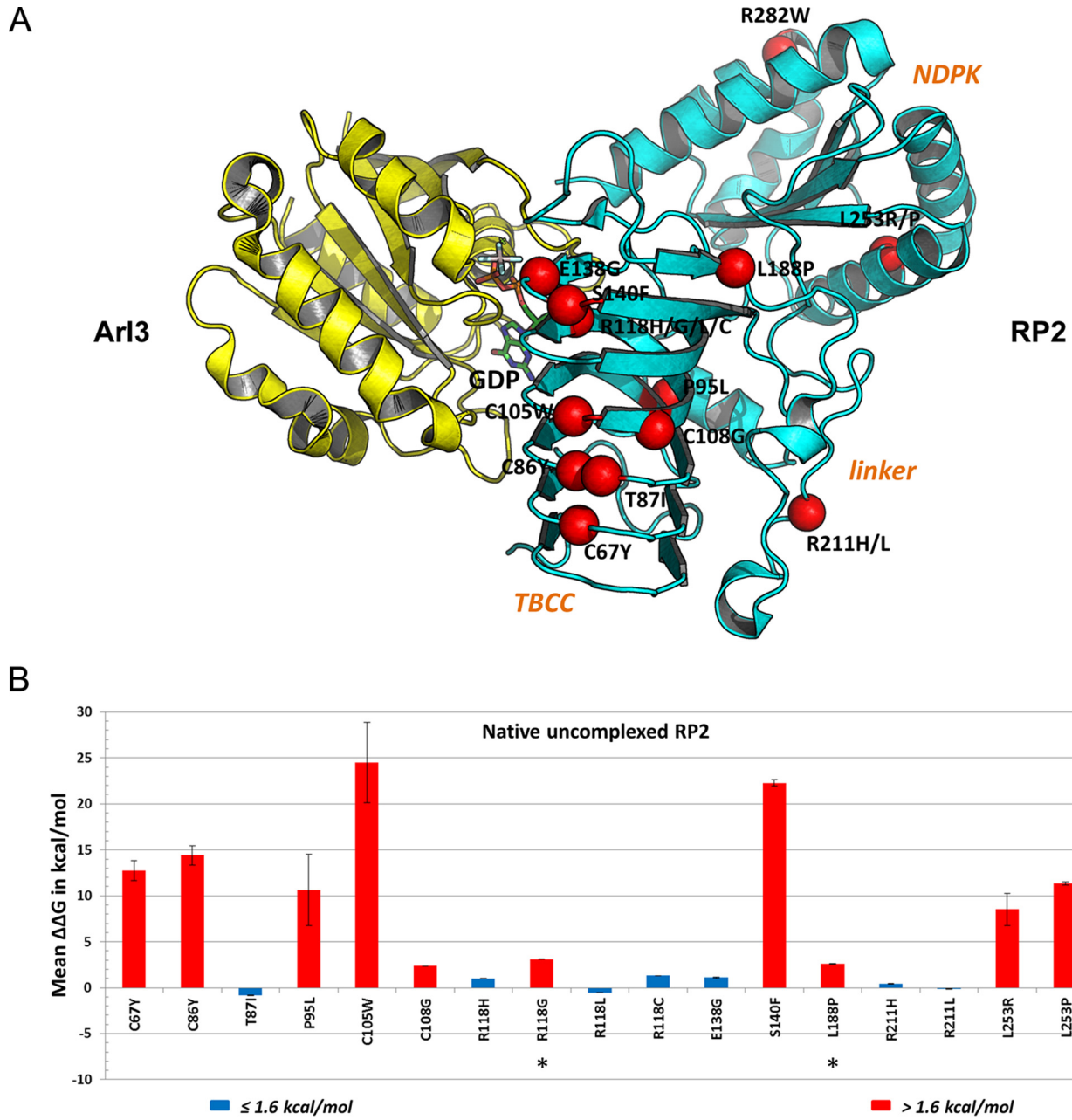

Figure 5. Structure-based modeling and analysis of *RP2* mutations. *A*, missense mutations mapped on RP2-Arl3 crystal structure. A schematic representation of the RP2 (*cyan*)-Arl3 (*yellow*) complex is shown along with GDP (*stick representation*, colored by atom type). The location of known disease-causing missense mutations is shown on RP2. Only the positions of the α carbon atoms are shown as *red spheres* and labeled. *B*, analysis of RP2 missense mutations on structure-function by FoldX. The calculated $\Delta\Delta G$ (kcal/mol) is shown as the mean of three calculation runs with standard error. $\Delta\Delta G \leq 1.6$ kcal/mol, no effect on structural stability (*blue*); $\Delta\Delta G > 1.6$ kcal/mol, severely reduced structural stability (*red*). Negative values indicate enhanced stabilities.

ARPE-19 cells (Fig. 6, *D* and *E*), suggesting that the entire C-terminal domain of RP2 is likely stable when expressed alone. The 251–350 truncation (missing the first 60 amino acids of 192–350 truncation) showed a markedly decreased protein level. This truncation is unstable probably due to the damage of the first β-strand (residues 234–240, β13 in Fig. 4*A*) and α-helix

Figure 4. More than half of the *RP2* missense mutations were destabilizing. *A*, the mutations investigated in this study are labeled in the alignment result of human and zebrafish RP2 protein sequences. *Red star*, missense mutations; *pink filled rectangle*, deletion mutations; *yellow box*, the del12 mutation; *green star*, polymorphism. *Red background*, strictly conserved positions; *red letter with white background*, conservatively substituted positions; *black letter with white background*, non-conserved positions. The secondary structures and solvent accessibility of each position are shown *above and below the alignment*. *Blue*, highly solvent-accessible; *cyan*, intermediate solvent-accessible; *white*, buried. *B*, 22 pathogenic forms of mutant RP2 proteins were expressed in ARPE-19 cells with a C-terminal GFP tag. Protein levels were detected by Western blot using the anti-GFP antibody. Tubulin was used as a loading control. The experiment shown was replicated at least three times. *C*, quantification of the data shown in *B*. The results are shown as mean with S.D. ($n = 5$). The protein levels of del12 and WT forms of RP2 are used as references to classify destabilizing and non-destabilizing mutations, respectively.

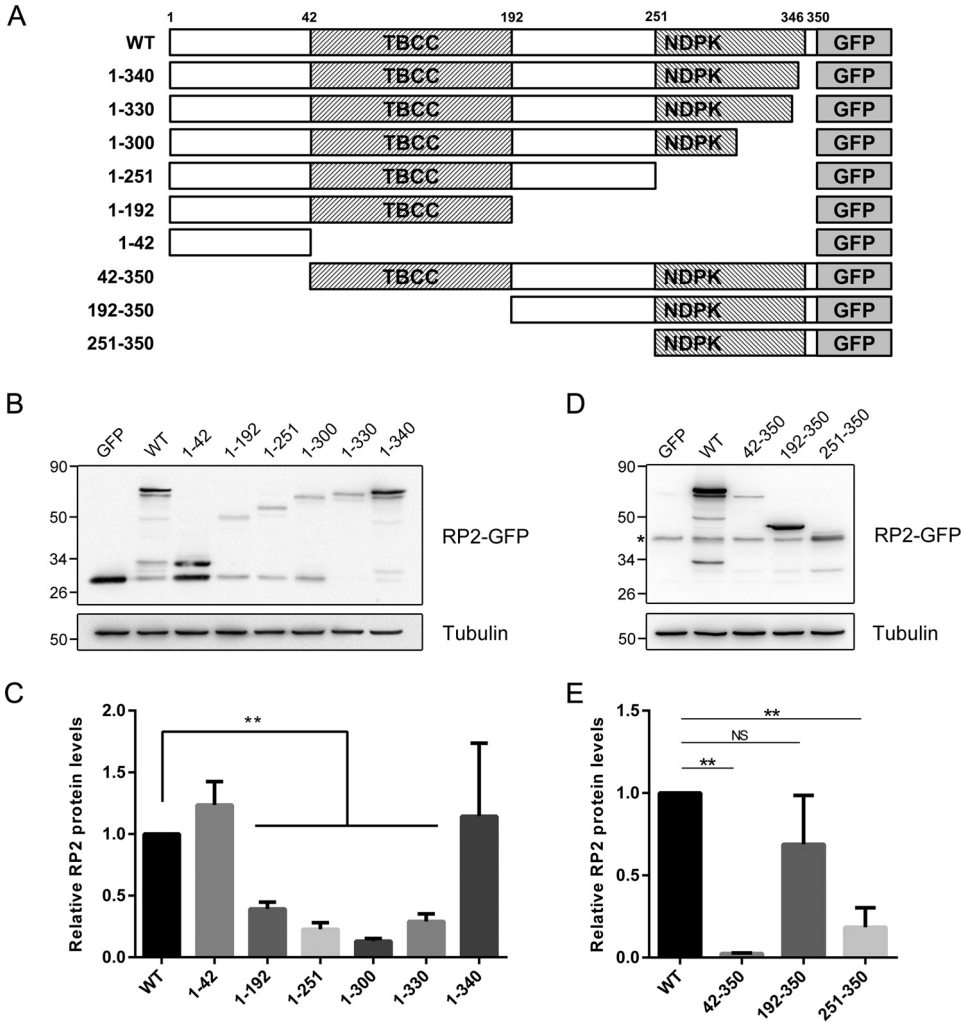

Figure 6. Expression levels of the C-terminal and N-terminal truncations of RP2. *A*, schematic diagram of the truncated RP2 proteins with a C-terminal GFP tag. The exact length of all studied truncations of RP2 is shown. *B* and *D*, the series of C-terminal truncated (*B*) and N-terminal truncated (*D*) RP2 were transfected into ARPE-19 cells, respectively. Their expression levels were determined by Western blot using either the anti-GFP antibody or the anti-RP2 antibody. Tubulin was used as a loading control. The experiment shown was replicated at least three times. *C* and *E*, the quantitative results of (*B* and *D*) are shown as the mean with S.D. ($n = 3$), correspondingly. **, $p < 0.01$; *NS*, non-significant.

(residues 246–259, α3 in Fig. 4*A*) of the C-terminal structure of RP2. Taken together our results demonstrate that *RP2* truncation mutations, which do not cause nonsense-mediated decay of mRNA, would still lead to destabilization and degradation of RP2 protein. In addition, the C-terminal NDPK domain of RP2, which probably has no enzymatic activity, might play an essential "structural" role in maintaining the global protein stability.

Destabilized RP2 proteins are degraded through the proteasome pathway

Protein destabilization can cause misfolded or even aggregated proteins, which is harmful and is cleared mainly through the proteasomal and lysosomal degradation pathways in eukaryotic cells (39). To determine the involved degradation pathway of the destabilized RP2 proteins, we treated the transfected cells with proteasomal and lysosomal inhibitors and then examined the protein levels of RP2 by Western blot. The proteasome inhibitors MG-132 and lactacystin both significantly restored the protein levels of del12 mutant RP2 (Fig. 7, *A* and *B*). In contrast, the lysosomal inhibitors chloroquine and leupeptin showed no effect (Fig. 7*A* and supplemental Fig. S7). To further confirm it, we repeated the experiments on those destabilizing pathogenic mutations and the N-terminal (42–350) and C-terminal (1–300) truncations. As expected, MG-132 treatment significantly increased the protein levels of P95L and 1–300 mutant forms of RP2 (Fig. 7, *C* and *D*) as well as the other destabilizing mutations (supplemental Fig. S8). These data suggest that the mutant RP2 proteins with significantly reduced stabilities are mainly degraded through the proteasome pathway.

Non-destabilizing mutations T87I and R211H do not affect the binding capacities of RP2 to ARL3 and GNB1

As for the remaining non-destabilizing mutations, R118H/R118G/R118L/R118C and E138G, which affect the residues buried at the interaction interface of RP2 and ARL3 (12), were previously predicted and validated to abolish the interaction. Expectedly, our pulldown assays also revealed that the R118G and E138G mutation reduced the strength of interaction between RP2 and ARL3 to ~10 and 40%, respectively (Fig. 8*A*). However, the highly solvent-accessible T87I and R211H muta-

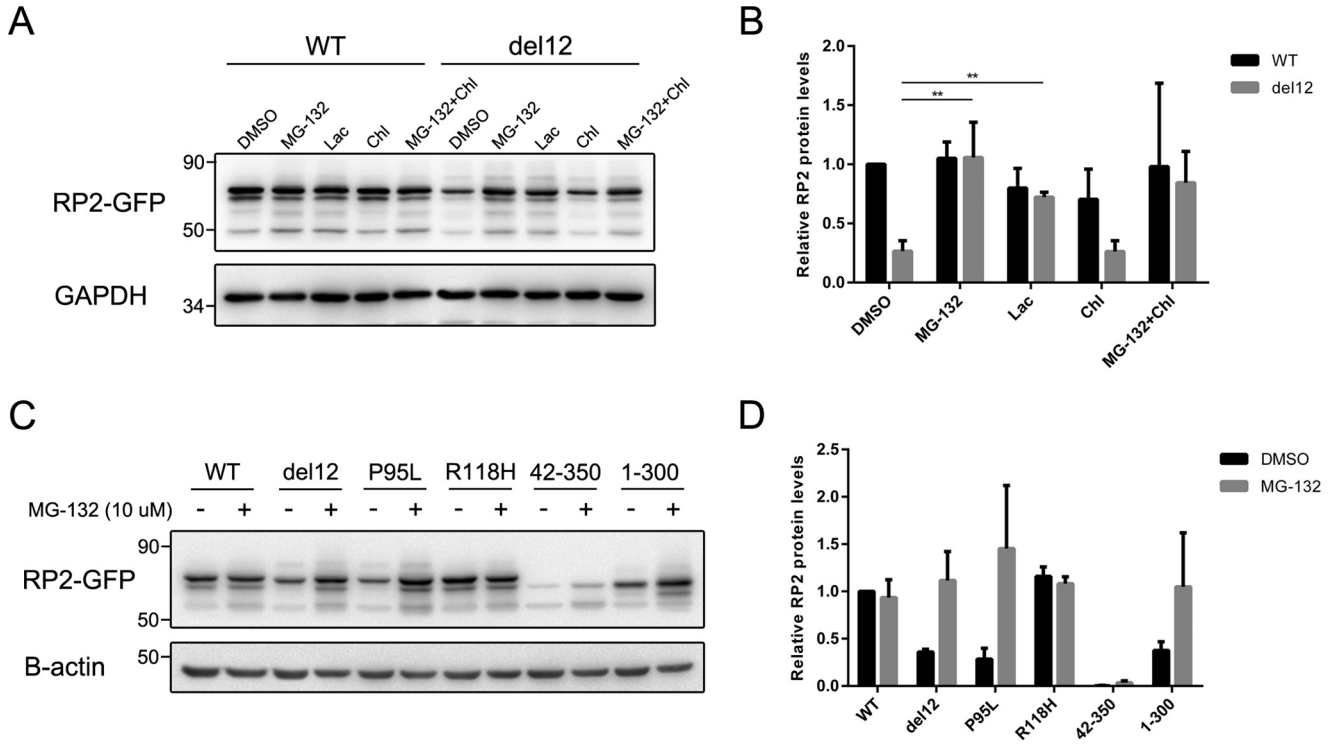

Figure 7. The unstable RP2 proteins were degraded through proteasome pathway in ARPE-19 cells. *A*, ARPE-19 cells transfected with WT and del12 mutant RP2 were treated with MG-132 (10 μM), lactacystin (Lac, 20 μM), or chloroquine (*Chl*, 20 μM) for 18 h. The RP2 protein levels were detected by Western blot. GAPDH was used as a loading control. The experiment shown was repeated at least three times. *B*, quantitative analysis of the Western blot data shown in *A* revealed that the proteasome inhibitors MG-132 and lactacystin significantly increased the protein levels of del12 mutant RP2. The results are shown as the mean with S.D. $n = 3$. **, $p < 0.01$. *C*, the P95L, 42–350, and 1–300 forms of RP2 were transfected into ARPE-19 cells, which were further treated with MG-132 (10 μM) for 18 h. RP2 protein levels were detected by Western blot. GAPDH was used as a loading control. The experiment shown was repeated at least three times. *D*, quantitative results of *C* from three independent experiments are shown as the mean with S.D. ($n = 3$). MG-132 treatment markedly increased the protein levels of P95L and 1–300 forms of RP2 mutants.

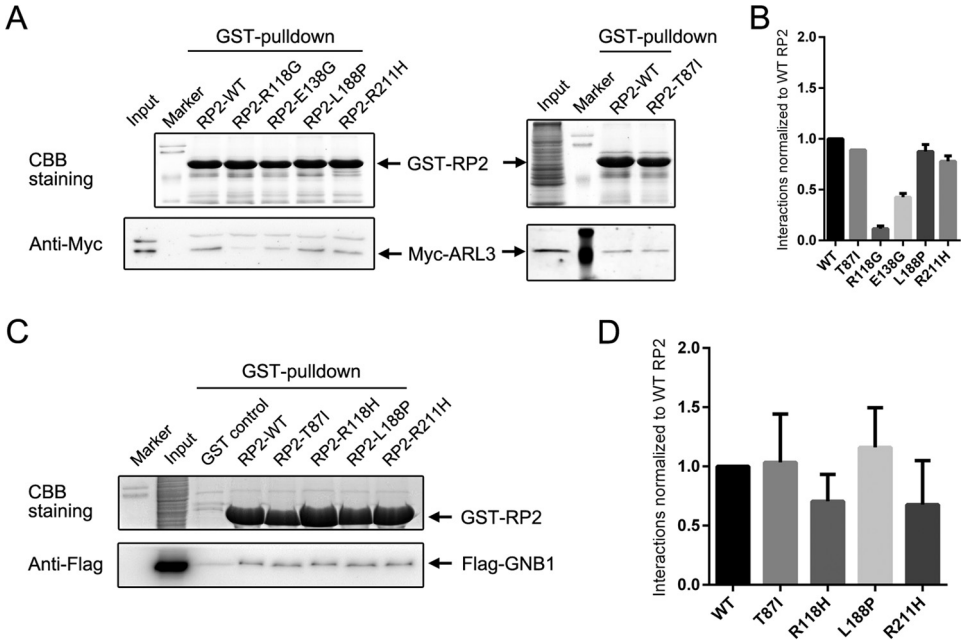

Figure 8. GST pulldown assays of the non-destabilizing and partly destabilized *RP2* mutations. *A* and *C*, pulldown results of WT and the indicated mutant forms of RP2 with Myc-tagged ARL3 (*A*) and FLAG-tagged GNB1 (*C*). Coomassie Brilliant Blue (*CBB*) staining shows the amounts of the immobilized GST-RP2 proteins. ARL3 and GNB1 are visualized by Western blot using corresponding antibodies. *B* and *D*, quantitative results of *A* and *C* are shown as the mean with S.D., respectively. The strength of the interaction is normalized to WT RP2 protein.

tions and the partly solvent-accessible L188P mutation showed no impact in the same experiments. To further identify the pathogenic effects of these mutations, we tested another important RP2 interacting protein, GNB1. Still, no obvious alteration was detected (Fig. 8*B*). These results indicate that loss of interaction with other proteins such as NSF (*N*-eth-

ylmaleimide-sensitive factor, vesicle fusing ATPase) (23), PKD2 (polycystin 2, transient receptor potential cation channel) (40), or unknown new partners might play a causal role for developing retinitis pigmentosa in patients carrying T87I and R211H/R211L mutations.

Discussion

Patients with *RP2* mutations usually show a rapid course of vision loss with decreased visual acuity at an early age (31). Several knockdown and knock-out animal models have been established to study the phenotypes and gene functions of *RP2* (4–7, 40–42). In this study we report a novel *rp2* mutant zebrafish line carrying an in-frame 12-bp deletion generated by TALEN technology. The protein levels of Rp2 in del12 homozygotes are extremely low, indicating a possible pathogenicity of the mutation. As expected, the rhodopsin kinase Grk1, the rod transducin subunits Gnat1 and Gnb1, and the β subunit of rod cGMP phosphodiesterase (Pde6b), are decreased in the del12 mutant zebrafish. In terms of retinal phenotypes, the del12 mutants show a slowly progressing retinal degeneration, which is likewise similar to the *rp2* knock-out zebrafish. As the mRNA level of del12 mutant *rp2* is only slightly reduced, over-degradation of the mutant protein might be the most reasonable explanation for the loss of Rp2 protein. Indeed, our *in vitro* expression tests, protein stability assay, and intraprotein interaction analysis based on the crystal structure of human RP2 demonstrate that the del12 mutation is highly destabilizing and will cause rapid degradation of the mutant RP2 protein.

More intriguingly, our experimental results indicate that in addition to the del12 mutation, more than half of the missense mutations (including single residue deletions) substantially decrease the protein stabilities and expression levels of RP2. The two highest resolution crystal structures of RP2 in Arl3-bound (resolution 1.9 Å) and unbound conformation (resolution 2.1 Å) were selected to perform *in silico* mutagenesis and stability calculations using the FoldX algorithm (35, 36), as was previously undertaken for mutations in rhodopsin (that also causes retinitis pigmentosa) (43) and for mutations in PAX6, a transcription factor involved in eye development and disease, such as aniridia (44). The resulting quantitative estimation of energy changes on the stability of the protein correlates well in both crystal structures and with our experimental data. To our knowledge this is the first report based on strict experiments that reveal a large proportion of the missense and small in-frame deletion mutations in *RP2* affect protein stabilities and protein levels.

How each of the mutations impact on the function of RP2 can be rationalized from our combined structure-based bioinformatics approach and experimental results. Mutations G2A, C3S, F5A, and S6del have been reported to impede the *N*-acylation of RP2 and interfere with its plasma membrane targeting previously (45, 46). More specifically, the G2A, F5A, and S6del mutant protein are not attached to any membranes, whereas the C3S mutant protein is associated with intracellular, but not plasma membranes (45). Interestingly, in our study the G2V, F5del, and S6del, but not C3S, are destabilizing, indicating the membrane association might be indispensable for RP2 protein stabilization. In addition, the observation that N-terminal truncation of RP2 lacking the first 41 amino acids (42–350) also shows an extremely low expression level (Fig. 6, *D* and *E*) is in agreement with the hypothesis.

Mutations C67Y, C86Y, P95L, C105W, C108G, I137del, S140F, L253R, and L253P, which cause notably reduced RP2 protein levels, are classified as destabilizing mutations in this study. The C67Y, C86Y, P95L, C108G, I137del, and L253R mutations were previously predicted to destabilize RP2 protein based on their locations (11), which are consistent with our *in silico* stability calculations and experimental data. All of the involved amino acid residues are buried in the hydrophobic core of the structure, including the previously unstudied Cys-105 and Ser-140. It is noteworthy that the Leu-253 is the only mutated residue located in the C-terminal NDPK domain of RP2.

Interestingly, L188P is suggested to be a destabilizing mutation by our *in silico* stability calculations and a previous prediction (11). Although the L188P mutant RP2 shows 60–70% expression levels relative to wild type RP2, its protein stability is obviously decreased as revealed by our DSF analysis (~11 °C reduction). This suggests that L188P is a destabilizing mutation substantially but not as severe as those destabilizing mutations mentioned above. In terms of structure, Leu-188 is located at the top of the final β-strand (residues 186–188) of the N-terminal TBCC domain and is in van der Waals contact with Trp-171 and Trp-186; importantly, the leucine aliphatic side chain interacts with the hydrophobic component of Arg-228 located in the linker region of RP2. These interactions will in part be compromised in L188P mutant RP2 protein, and therefore, a local destabilization effect is possible even though the mutant protein is expressed relatively well. In addition, the loss of the interdomain interaction between Leu-188 and Arg-228 allows greater flexibility between the TBCC and linker-NDPK domains, which may affect potential protein-protein interactions that rely on more than one domain.

Mutations T87I, R118H/R118G/R118L/R118C, E138G, and R211H/R211L on the other hand are identified as non-destabilizing mutations in our study. Previously undertaken circular dichroism spectra of R118H and E138G mutant RP2 proteins confirmed that they have no impact on the secondary structure content and hence no effect on the overall folding of the mutant proteins (11). Our experiments suggest that R118G and E138G show very slight destabilizing effects (<5 °C reductions in DSF analysis) and near normal expression levels. Probably, the mild destabilizing effects are insufficient to cause severe misfolding and degradation of the mutant RP2 proteins. According to the crystal structure, the side chains of these affected residues are highly surface-exposed and, therefore, might not contribute to the overall stability of RP2 protein.

For these non-destabilizing mutations, alteration of protein-protein interaction is the likely cause of disease. It is already known that R118H and E138G weaken the binding capacity of RP2 to ARL3 and thus prevent the activation of ARL3 GTPase (11, 12). Our GST pulldown assays also show that R118G and E138G reduce the interaction between RP2 and ARL3. The Arg-118 residue of RP2 has been suggested to act as an "arginine finger" within the common conserved active site found in GAPs (10), suggesting that the other two mutations (R118C and R118L) affecting the same residue are likely to abolish the GAP activity of RP2 as well. The T87I and R211H mutant forms of

RP2 interact normally with ARL3 and GNB1 in our GST pulldown assays, indicating that impaired interaction(s) with other RP2 partners such as NSF (23) and polycystin 2 (PKD2) (40) might be the pathogenic effect of these mutations.

C-terminal-truncated mutations account for ~2/3 cases of RP2 patients. Our work indicates that except nonsense-mediated decay, destabilization and degradation of the C-terminal-truncated RP2 protein is another cause of pathogenicity for truncation mutations in *RP2*. According to the crystal structure of RP2 (11, 12), the C-terminal domain (residues 229–347) of RP2 forms a three-layered $\alpha+\beta$ sandwich with an antiparallel β-sheet surrounded by 4 α-helices and a short 3_{10}-helix on both sides. The 1–340 truncation retains nearly the entire $\alpha+\beta$ sandwich structure and is stable, whereas the 1–330 truncation that lacked the last α-helix (residues 330–345, α6 in Fig. 4*A*) is unstable, suggesting that a full conformation of the C-terminal domain is crucial for the overall stability of RP2 protein.

In conclusion we report a novel zebrafish line with an in-frame 12-bp deletion in *rp2*. Loss of protein stability is the main consequence of the del12 mutation, which further leads to retinal degeneration. In addition, more than half of missense and single-residue deletion mutations and the C-terminal truncation mutations identified in RP2 patients are destabilizing. The destabilized RP2 proteins are degraded through the proteasome pathway. For the first time our study comprehensively characterizes the disease-causing mutations in *RP2* and provides robust evidence to indicate that loss of RP2 protein stability but not alteration of its molecular function (except for T87I, R118H/R118G/R118L/R118C, E138G, and R211H/R211L) is probably the major pathogenic cause for most *RP2* mutations. Our study also reveals a role of the C-terminal domain of RP2 in maintaining the overall protein stability. Further studies are needed to elucidate how T87I and R211H/R211L alter the function of RP2 and how loss of RP2 protein causes retinal degeneration.

Experimental Procedures

Zebrafish maintenance and genotyping

Wild type and mutant zebrafish were maintained and bred as described previously (7). The del12 mutant zebrafish were screened out by the PCR-restriction fragment length polymorphism (PCR-RFLP) method. Briefly, a 574-bp DNA fragment was amplified (forward, 5′-tgcggtatcgatgctgaaatga-3′; reverse, 5′-ggcgcagcacaaaaagacgt-3′) using genomic DNA isolated from tail fin and digested with MspI (New England BioLabs) at 37 °C for 4 h. The native MspI restriction site will be disrupted by the del12 mutation, which leads to an uncut band in DNA gel electrophoresis. The homozygotes were further confirmed by DNA sequencing. Zebrafish with similar body sizes at the same ages form different genotype groups were randomly selected and included in the study. All procedures involving zebrafish were approved by the Ethics Committee of Huazhong University of Science and Technology and were in accordance with the ARRIVE guidelines.

Site-directed mutagenesis and vector construction

Full-length human *RP2* coding sequence was amplified from the cDNA of ARPE-19 cells. *RP2* mutations were generated by overlap extension PCR-mediated site-directed mutagenesis. WT and mutant *RP2* were cloned into the pEGFPN1 (Clontech) and pcDNA3.1 (Invitrogen) vectors for eukaryotic expression of C-terminal GFP and FLAG-tagged protein, respectively. For prokaryotic expression, the WT, del12, P95L, and R118H forms of *RP2* were cloned into the pGEX-4T-1 vector (GE Healthcare). All plasmids were confirmed by DNA sequencing.

Cell culture, transfection, and inhibitor treatment

The ARPE-19 (ATCC catalog #CRL-2302), HepG2 (ATCC catalog #HB-8065), and H1299 (ATCC catalog #CRL-5803) cell lines were purchased from ATCC (American Type Culture Collection). DAPI staining of each cell line was performed to examine the status of mycoplasma contamination. Cells were cultured under recommended conditions. In brief cells were placed in DMEM medium (HepG2 and H1299) or DMEM:F-12 medium (ARPE-19) containing 10% fetal bovine serum and incubated at 37 °C in 5% CO_2 in a humidified incubator. When grown to 80–90% confluence, cells were re-plated at a split ratio of 1:3~1:5. Cell transfection was performed using Lipofectamine 3000 (Invitrogen) according to the manual. For inhibitor treatment, after transfection, cells were cultured for 18 h with designated concentrations of MG-132 (10 μM), lactacystin (20 μM, Sigma), chloroquine (20 μM, Sigma), or leupeptin (250 μM, Selleck).

Protein purification, differential scanning fluorimetry, and GST pulldown

Expression of GST-tagged RP2 proteins were performed in BL21 strain following the handbook of GST Gene Fusion System (GE Healthcare). *E. coli* cells were induced with 0.1 mM isopropyl 1-thio-β-D-galactopyranoside at 25 °C for 4 h. After that, cells were harvested and lysed in PBS buffer containing 0.1% Triton X-100 and 1 mM PMSF by sonication. The lysates were centrifuged at 4 °C, 12,000 rpm for 20 min to separate the soluble (supernatant) and insoluble (precipitate) components. Glutathione beads (Thermo Fisher Scientific) were added to the supernatants and rotated at 4 °C for 4 h. GST fusion protein was eluted with elution buffer (50 mM Tris, pH 8.0, 20 mM reduced glutathione) by rotating at 4 °C for 1 h. The supernatant, precipitate, and purified protein were examined by SDS-PAGE and Coomassie Blue staining. DSF (47) was performed to detect the thermal stabilities of these purified proteins using the Protein Thermal Shift™ Dye kit (Applied Biosystems) on the StepOnePlus™ real-time PCR System (Applied Biosystems). The data were analyzed by the Protein Thermal Shift Software 1.3 (Thermo Fisher Scientific). For GST-pulldown, cell lysates expressing ARL3-Q71L (GTP-bound form) or GNB1 were incubated with immobilized RP2 proteins on glutathione beads for 4 h at 4 °C. After washing the beads with lysis buffer for 3–4 times, the bound proteins were eluted and analyzed by Western blot.

Western blot and immunofluorescence staining

Zebrafish were sacrificed by immersing in 0.02% MS222 (Sigma) solution for 15 min or until no opercular movement. For protein preparation, eyes were enucleated and sonicated in radioimmune precipitation assay lysis buffer containing protease inhibitor mixture (Sigma). Cultured cells were washed twice

with cold PBS and lysed with the same radioimmune precipitation assay buffer. Protein concentrations were determined using the BCA Protein Assay kit (Beyotime, Shanghai, China). Western blot was performed as described previously (48). The membranes were developed using the ChemiDoc XRS+ imaging system (Bio-Rad). Gray intensity analysis of bands was performed by the Quantity One 4.62 software. The immunostaining of zebrafish retina sections was performed as described previously (7). Fluorescence images were acquired on the FluoView™ FV1000 confocal laser-scanning microscope (Olympus). The following primary antibodies were used in this study: the anti-zebrafish Rp2 antibody (1:1000 for WB, 1:50 for immunofluorescence (IF)) (7), the anti-rhodopsin 4D2 antibody (1:200 for IF; Abcam, ab183399), PNA (50 μg/ml for IF; Molecular Probes, L21409), the anti-RP2 antibody (1:1000 for WB; Abclonal, A3212), the anti-Pde6b antibody (1:500 for WB, Proteintech, 22063-1-AP), the anti-GRK1 antibody (1:1000 for WB; Abclonal, A6497), the anti-GNAT1 antibody (1:500 for WB; Proteintech, 55167-1-AP), the anti-GNB1 antibody (1:1000 for WB; Abgent, AP5036a), the anti-GNB3 antibody (1:1000 for WB; Proteintech, 10081-1-AP), the anti-ARL3 antibody (1:200 for WB; Abclonal, A6499), the anti-NSF antibody (1:1000 for WB; Abclonal, A0926), the anti-GAPDH antibody (1:3000 for WB; Abclonal, AC001), the anti-GFP antibody (1:5000 for WB; Abmart, M20004), the anti-FLAG antibody (1:5000 for WB; MBL, M185), the anti-α tubulin antibody (1:5000 for WB; Millipore, CP06), the anti-β actin antibody (1:2000 for WB; Proteintech, 60008–1-Ig).

RT-qPCR

RNAs were isolated using RNAiso Plus reagent (Takara) from at least three zebrafish eyes for each sample. Reverse transcription was performed using MMLV reverse transcriptase (Invitrogen) and oligo(dT) primer (Takara). The mRNA levels of WT and mutant *rp2* were detected on the StepOnePlus™ real-time PCR System (Applied Biosystems) using AceQ™ qPCR SYBR Green Master Mix (Vazyme Biotech, Nanjing, China). The data were analyzed using StepOne software (version 2.3), and significance was determined by two-tailed Student's *t* test. Primer sequences were reported in our previous studies (7).

Ultrastructural analysis

Zebrafish eyes were fixed (2.5% glutaraldehyde, 0.1 M PBS buffer, pH 7.0) overnight at 4 °C. After 3 washes with PBS, the eyes were further fixed in 1% osmium tetroxide for 2 h at room temperature and dehydrated in a 50, 70, 80, 90, 95, and 100% ethanol series. The eyes were incubated in acetone for 20 min, treated with 50% (1 h), 75% (3 h), and 100% (overnight) epoxy resin (mixed with acetone, v/v), and then heated at 70 °C overnight. Embedded eyes were sliced to ultrathin sections (70 nm) using an Reichert-Jung ultramicrotome (Leica). Sections were stained with 3% uranyl acetate and 3% lead citrate for 15 min and visualized with a transmission electron microscope system (HT7700, Hitachi).

Structure-based modeling analysis of RP2 mutations

The X-ray crystal structures of both native (uncomplexed) human RP2 (PDB ID 2BX6, resolution 2.1 Å) (11) and RP2 in complex with Arl3 (PDB ID 3BH7, resolution 1.9 Å) (12) have been solved and were analyzed independently. The empirical forcefield FoldX version 4 (35, 36) was used to estimate the free energy difference *i.e.* stability change upon mutagenesis from wild type ($\Delta\Delta G$) and also to perform interaction energy calculations upon mutation in the complexed RP2 structure. In brief, amino acid residues with missing side-chain atoms, Van der Waals clashes, with bad torsion angles, or with a high energy in the crystal structure were repaired by replacing the side chain conformations (rotamers) observed in the X-ray structures by lower energy rotamers. This was achieved using the RepairPDB option, which also optimized the hydrogen bond networks (35, 36). After energy minimization, the BuildModel option was used to calculate the stability change using the following parameters (number of runs, 3; pH 7; temperature 298 K; ionic strength 0.05 M; VdW design, 2). Where mutations were present at or near the interface with Arl3/GDP, the potential change in interaction energy was determined using the "PSSM" option (number of runs: 3) that incorporates the BuildModel and AnalyseComplex commands. All resulting energies are expressed in kcal/mol. The error margin of FoldX is ~0.5 kcal/mol (35) so changes in that range are considered insignificant. The prediction decision on whether the mutation destabilizes the structure is based upon Refs. 36, 43 and 49), where no effect on structural stability $\Delta\Delta G$ is $\leq$1.6 kcal/mol, and severely reduced structural stability $\Delta\Delta G$ is $>$1.6 kcal/mol. Intraprotein interactions of the four residues affected by the del12 mutation were analyzed using the Protein Interactions Calculator (PIC) server (26). ESPript version 3 (50) was used to annotate the alignment.

Statistical analysis

Two-sided Student's *t* test was performed with a 95% confidence level to determine the statistical significance between two groups using the GraphPad Prism 6 software. All data are presented as mean with S.D. * represents $p < 0.05$; ** represents $p < 0.01$.

Author contributions—M. L. developed the concept of this study. F. L. and Y. Q. designed the study and performed most of the experiments in zebrafish and cell lines and analyzed the data. S. Y. performed the generation of rp2 mutant zebrafish by TALEN technology. D. C. S. undertook the structure-based analysis and *in silico* stability calculations of mutant RP2 proteins. L. Y. contributed invector construction and Western blot. C. L., M. G., and X. H. helped in ARPE-19 cell culture and GST-pulldown assays. Z. L. and X. L. helped in the preparation of zebrafish retinal sections. J. W., X. S., Z. T., J. Y. L., and T. J. revised the manuscript critically for important intellectual content. F. L., D. C. S., and M. L. prepared the draft and final version of the manuscript. All authors reviewed the results and approved the manuscript.

Acknowledgment—We thank Luying Liu for kind help in revising the manuscript for language.

References

1. Hartong, D. T., Berson, E. L., and Dryja, T. P. (2006) Retinitis pigmentosa. *Lancet* **368,** 1795–1809

2. Prokisch, H., Hartig, M., Hellinger, R., Meitinger, T., and Rosenberg, T. (2007) A population-based epidemiological and genetic study of X-linked retinitis pigmentosa. *Invest. Ophthalmol. Vis. Sci.* **48,** 4012–4018
3. Pelletier, V., Jambou, M., Delphin, N., Zinovieva, E., Stum, M., Gigarel, N., Dollfus, H., Hamel, C., Toutain, A., Dufier, J. L., Roche, O., Munnich, A., Bonnefont, J. P., Kaplan, J., and Rozet, J. M. (2007) Comprehensive survey of mutations in RP2 and RPGR in patients affected with distinct retinal dystrophies: genotype-phenotype correlations and impact on genetic counseling. *Hum. Mutat.* **28,** 81–91
4. Li, L., Khan, N., Hurd, T., Ghosh, A. K., Cheng, C., Molday, R., Heckenlively, J. R., Swaroop, A., and Khanna, H. (2013) Ablation of the X-linked retinitis pigmentosa 2 (Rp2) gene in mice results in opsin mislocalization and photoreceptor degeneration. *Invest. Ophthalmol. Vis. Sci.* **54,** 4503–4511
5. Zhang, H., Hanke-Gogokhia, C., Jiang, L., Li, X., Wang, P., Gerstner, C. D., Frederick, J. M., Yang, Z., and Baehr, W. (2015) Mistrafficking of prenylated proteins causes retinitis pigmentosa 2. *FASEB J.* **29,** 932–942
6. Li, L., Rao, K. N., Zheng-Le, Y., Hurd, T. W., Lillo, C., and Khanna, H. (2015) Loss of retinitis pigmentosa 2 (RP2) protein affects cone photoreceptor sensory cilium elongation in mice. *Cytoskeleton* **72,** 447–454
7. Liu, F., Chen, J., Yu, S., Raghupathy, R. K., Liu, X., Qin, Y., Li, C., Huang, M., Liao, S., Wang, J., Zou, J., Shu, X., Tang, Z., and Liu, M. (2015) Knockout of RP2 decreases GRK1 and rod transducin subunits and leads to photoreceptor degeneration in zebrafish. *Hum. Mol. Genet.* **24,** 4648–4659
8. Schwahn, U., Lenzner, S., Dong, J., Feil, S., Hinzmann, B., van Duijnhoven, G., Kirschner, R., Hemberger, M., Bergen, A. A., Rosenberg, T., Pinckers, A. J., Fundele, R., Rosenthal, A., Cremers, F. P., Ropers, H. H., and Berger, W. (1998) Positional cloning of the gene for X-linked retinitis pigmentosa 2. *Nat. Genet.* **19,** 327–332
9. Miano, M. G., Testa, F., Filippini, F., Trujillo, M., Conte, I., Lanzara, C., Millán, J. M., De Bernardo, C., Grammatico, B., Mangino, M., Torrente, I., Carrozzo, R., Simonelli, F., Rinaldi, E., Ventruto, V., D'Urso, M., Ayuso, C., and Ciccodicola, A. (2001) Identification of novel RP2 mutations in a subset of X-linked retinitis pigmentosa families and prediction of new domains. *Hum. Mutat.* **18,** 109–119
10. Evans, R. J., Hardcastle, A. J., and Cheetham, M. E. (2006) Focus on molecules: X-linked retinitis pigmentosa 2 protein, RP2. *Exp. Eye Res.* **82,** 543–544
11. Kühnel, K., Veltel, S., Schlichting, I., and Wittinghofer, A. (2006) Crystal structure of the human retinitis pigmentosa 2 protein and its interaction with Arl3. *Structure* **14,** 367–378
12. Veltel, S., Gasper, R., Eisenacher, E., and Wittinghofer, A. (2008) The retinitis pigmentosa 2 gene product is a GTPase-activating protein for Arf-like 3. *Nat. Struct. Mol. Biol.* **15,** 373–380
13. Bartolini, F., Bhamidipati, A., Thomas, S., Schwahn, U., Lewis, S. A., and Cowan, N. J. (2002) Functional overlap between retinitis pigmentosa 2 protein and the tubulin-specific chaperone cofactor C. *J. Biol. Chem.* **277,** 14629–14634
14. Schwarz, N., Novoselova, T. V., Wait, R., Hardcastle, A. J., and Cheetham, M. E. (2012) The X-linked retinitis pigmentosa protein RP2 facilitates G protein traffic. *Hum. Mol. Genet.* **21,** 863–873
15. Wright, K. J., Baye, L. M., Olivier-Mason, A., Mukhopadhyay, S., Sang, L., Kwong, M., Wang, W., Pretorius, P. R., Sheffield, V. C., Sengupta, P., Slusarski, D. C., and Jackson, P. K. (2011) An ARL3-UNC119-RP2 GTPase cycle targets myristoylated NPHP3 to the primary cilium. *Genes Dev.* **25,** 2347–2360
16. Wright, Z. C., Singh, R. K., Alpino, R., Goldberg, A. F., Sokolov, M., and Ramamurthy, V. (2016) ARL3 regulates trafficking of prenylated phototransduction proteins to the rod outer segment. *Hum. Mol. Genet.* **25,** 2031–2044
17. Hanke-Gogokhia, C., Wu, Z., Gerstner, C. D., Frederick, J. M., Zhang, H., and Baehr, W. (2016) Arf-like protein 3 (ARL3) regulates protein trafficking and ciliogenesis in mouse photoreceptors. *J. Biol. Chem.* **291,** 7142–7155
18. Yoon, J. H., Qiu, J., Cai, S., Chen, Y., Cheetham, M. E., Shen, B., and Pfeifer, G. P. (2006) The retinitis pigmentosa-mutated RP2 protein exhibits exonuclease activity and translocates to the nucleus in response to DNA damage. *Exp. Cell Res.* **312,** 1323–1334
19. Stenson, P. D., Mort, M., Ball, E. V., Shaw, K., Phillips, A., and Cooper, D. N. (2014) The Human Gene Mutation Database: building a comprehensive mutation repository for clinical and molecular genetics, diagnostic testing and personalized genomic medicine. *Hum. Genet.* **133,** 1–9
20. Mears, A. J., Gieser, L., Yan, D., Chen, C., Fahrner, S., Hiriyanna, S., Fujita, R., Jacobson, S. G., Sieving, P. A., and Swaroop, A. (1999) Protein-truncation mutations in the RP2 gene in a North American cohort of families with X-linked retinitis pigmentosa. *Am. J. Hum. Genet.* **64,** 897–900
21. Grayson, C., Chapple, J. P., Willison, K. R., Webster, A. R., Hardcastle, A. J., and Cheetham, M. E. (2002) *In vitro* analysis of aminoglycoside therapy for the Arg120stop nonsense mutation in RP2 patients. *J. Med. Genet.* **39,** 62–67
22. Baehr, W. (2014) Membrane protein transport in photoreceptors: the function of PDEδ: the Proctor lecture. *Invest. Ophthalmol. Vis. Sci.* **55,** 8653–8666
23. Holopainen, J. M., Cheng, C. L., Molday, L. L., Johal, G., Coleman, J., Dyka, F., Hii, T., Ahn, J., and Molday, R. S. (2010) Interaction and localization of the retinitis pigmentosa protein RP2 and NSF in retinal photoreceptor cells. *Biochemistry* **49,** 7439–7447
24. Sharon, D., Bruns, G. A., McGee, T. L., Sandberg, M. A., Berson, E. L., and Dryja, T. P. (2000) X-linked retinitis pigmentosa: mutation spectrum of the RPGR and RP2 genes and correlation with visual function. *Invest. Ophthalmol. Vis. Sci.* **41,** 2712–2721
25. Schwahn, U., Paland, N., Techritz, S., Lenzner, S., and Berger, W. (2001) Mutations in the X-linked RP2 gene cause intracellular misrouting and loss of the protein. *Hum. Mol. Genet.* **10,** 1177–1183
26. Tina, K. G., Bhadra, R., and Srinivasan, N. (2007) PIC: Protein Interactions Calculator. *Nucleic Acids Res.* **35,** W473–W476
27. Neidhardt, J., Glaus, E., Lorenz, B., Netzer, C., Li, Y., Schambeck, M., Wittmer, M., Feil, S., Kirschner-Schwabe, R., Rosenberg, T., Cremers, F. P., Bergen, A. A., Barthelmes, D., Baraki, H., Schmid, F., *et al.* (2008) Identification of novel mutations in X-linked retinitis pigmentosa families and implications for diagnostic testing. *Mol. Vis.* **14,** 1081–1093
28. Breuer, D. K., Yashar, B. M., Filippova, E., Hiriyanna, S., Lyons, R. H., Mears, A. J., Asaye, B., Acar, C., Vervoort, R., Wright, A. F., Musarella, M. A., Wheeler, P., MacDonald, I., Iannaccone, A., Birch, D., *et al.* (2002) A comprehensive mutation analysis of RP2 and RPGR in a North American cohort of families with X-linked retinitis pigmentosa. *Am. J. Hum. Genet.* **70,** 1545–1554
29. Beltran, W. A., Hammond, P., Acland, G. M., and Aguirre, G. D. (2006) A frameshift mutation in RPGR exon ORF15 causes photoreceptor degeneration and inner retina remodeling in a model of X-linked retinitis pigmentosa. *Invest. Ophthalmol. Vis. Sci.* **47,** 1669–1681
30. Wada, Y., Nakazawa, M., Abe, T., and Tamai, M. (2000) A new Leu253Arg mutation in the RP2 gene in a Japanese family with X-linked retinitis pigmentosa. *Invest. Ophthalmol. Vis. Sci.* **41,** 290–293
31. Jayasundera, T., Branham, K. E., Othman, M., Rhoades, W. R., Karoukis, A. J., Khanna, H., Swaroop, A., and Heckenlively, J. R. (2010) RP2 phenotype and pathogenetic correlations in X-linked retinitis pigmentosa. *Arch. Ophthalmol.* **128,** 915–923
32. Bader, I., Brandau, O., Achatz, H., Apfelstedt-Sylla, E., Hergersberg, M., Lorenz, B., Wissinger, B., Wittwer, B., Rudolph, G., Meindl, A., and Meitinger, T. (2003) X-linked retinitis pigmentosa: RPGR mutations in most families with definite X linkage and clustering of mutations in a short sequence stretch of exon ORF15. *Invest. Ophthalmol. Vis. Sci.* **44,** 1458–1463
33. Villaverde-Montero, C., Garcia-Hoyos, M., Gimenez-Pardo, A., Trujillo-Tiebas, M. J., Baiget, M., and Ayuso, C. (2007) Gene symbol: RP2. *Hum. Genet.* **121,** 289
34. Thiselton, D. L., Zito, I., Plant, C., Jay, M., Hodgson, S. V., Bird, A. C., Bhattacharya, S. S., and Hardcastle, A. J. (2000) Novel frameshift mutations in the RP2 gene and polymorphic variants. *Hum. Mutat.* **15,** 580
35. Schymkowitz, J., Borg, J., Stricher, F., Nys, R., Rousseau, F., and Serrano, L. (2005) The FoldX web server: an online force field. *Nucleic Acids Res.* **33,** W382–W388
36. Guerois, R., Nielsen, J. E., and Serrano, L. (2002) Predicting changes in the stability of proteins and protein complexes: a study of more than 1000 mutations. *J. Mol. Biol.* **320,** 369–387

37. Dandekar, S. S., Ebenezer, N. D., Grayson, C., Chapple, J. P., Egan, C. A., Holder, G. E., Jenkins, S. A., Fitzke, F. W., Cheetham, M. E., Webster, A. R., and Hardcastle, A. J. (2004) An atypical phenotype of macular and peripapillary retinal atrophy caused by a mutation in the RP2 gene. *Br. J. Ophthalmol.* **88,** 528–532
38. Pomares, E., Riera, M., Castro-Navarro, J., Andrés-Gutiérrez, A., Gonzàlez-Duarte, R., and Marfany, G. (2009) Identification of an intronic single-point mutation in RP2 as the cause of semidominant X-linked retinitis pigmentosa. *Invest. Ophthalmol. Vis. Sci.* **50,** 5107–5114
39. Balchin, D., Hayer-Hartl, M., and Hartl, F. U. (2016) In vivo aspects of protein folding and quality control. *Science* **353,** aac4354
40. Hurd, T., Zhou, W., Jenkins, P., Liu, C. J., Swaroop, A., Khanna, H., Martens, J., Hildebrandt, F., and Margolis, B. (2010) The retinitis pigmentosa protein RP2 interacts with polycystin 2 and regulates cilia-mediated vertebrate development. *Hum. Mol. Genet.* **19,** 4330–4344
41. Shu, X., Zeng, Z., Gautier, P., Lennon, A., Gakovic, M., Cheetham, M. E., Patton, E. E., and Wright, A. F. (2011) Knockdown of the zebrafish ortholog of the retinitis pigmentosa 2 (RP2) gene results in retinal degeneration. *Invest. Ophthalmol. Vis. Sci.* **52,** 2960–2966
42. Patil, S. B., Hurd, T. W., Ghosh, A. K., Murga-Zamalloa, C. A., and Khanna, H. (2011) Functional analysis of retinitis pigmentosa 2 (RP2) protein reveals variable pathogenic potential of disease-associated missense variants. *PLoS ONE* **6,** e21379
43. Rakoczy, E. P., Kiel, C., McKeone, R., Stricher, F., and Serrano, L. (2011) Analysis of disease-linked rhodopsin mutations based on structure, function, and protein stability calculations. *J. Mol. Biol.* **405,** 584–606
44. Alibés, A., Nadra, A. D., De Masi, F., Bulyk, M. L., Serrano, L., and Stricher, F. (2010) Using protein design algorithms to understand the molecular basis of disease caused by protein-DNA interactions: the Pax6 example. *Nucleic Acids Res.* **38,** 7422–7431
45. Chapple, J. P., Hardcastle, A. J., Grayson, C., Willison, K. R., and Cheetham, M. E. (2002) Delineation of the plasma membrane targeting domain of the X-linked retinitis pigmentosa protein RP2. *Invest. Ophthalmol. Vis. Sci.* **43,** 2015–2020
46. Chapple, J. P., Hardcastle, A. J., Grayson, C., Spackman, L. A., Willison, K. R., and Cheetham, M. E. (2000) Mutations in the N terminus of the X-linked retinitis pigmentosa protein RP2 interfere with the normal targeting of the protein to the plasma membrane. *Hum. Mol. Genet.* **9,** 1919–1926
47. Niesen, F. H., Berglund, H., and Vedadi, M. (2007) The use of differential scanning fluorimetry to detect ligand interactions that promote protein stability. *Nat. Protoc.* **2,** 2212–2221
48. Li, C., Wang, L., Zhang, J., Huang, M., Wong, F., Liu, X., Liu, F., Cui, X., Yang, G., Chen, J., Liu, Y., Wang, J., Liao, S., Gao, M., Hu, X., Shu, X., Wang, Q., Yin, Z., Tang, Z., and Liu, M. (2014) CERKL interacts with mitochondrial TRX2 and protects retinal cells from oxidative stress-induced apoptosis. *Biochim. Biophys. Acta* **1842,** 1121–1129
49. Tokuriki, N., Stricher, F., Schymkowitz, J., Serrano, L., and Tawfik, D. S. (2007) The stability effects of protein mutations appear to be universally distributed. *J. Mol. Biol.* **369,** 1318–1332
50. Robert, X., and Gouet, P. (2014) Deciphering key features in protein structures with the new ENDscript server. *Nucleic Acids Res.* **42,** W320–W324